PHILOSOPHICAL TRANSACTIONS OF THE ROYAL SOCIETY A MATHEMATICAL, PHYSICAL & ENGINEERING SCIENCES

A Phenomenological Model for Frictional Contact Accounting for Wear Effects

E. A. De Souza Neto, K. Hashimoto, Djordje Peric and D. R. J. Owen

Phil. Trans. R. Soc. Lond. A 1996 **354**, 819-843
doi: 10.1098/rsta.1996.0034

A phenomenological model for frictional contact accounting for wear effects

By E. A. de Souza Neto, K. Hashimoto†, Djordje Perić and D. R. J. Owen

Department of Civil Engineering, University of Wales Swansea, Singleton Park, Swansea SA2 8PP, UK

Contents

A simple phenomenological model for frictional contact accounting for wear effects is proposed. The objective is the numerical simulation of the frictional behaviour of contacting bodies subjected to large sliding distances and variable normal pressures. Within the context of thermodynamics with internal variables, the friction coefficient is assumed to be a function of the density of frictional work resulting in a theory analogous to classical work hardening elastoplasticity. The technique for experimental identification of the proposed model, applied to sheet materials, is described and the material parameters for some steel sheets commonly used in industry are determined. The framework for the computer simulation of the model in large scale problems is based on a fully implicit finite-element scheme and the Newton–Raphson method. A robust algorithm based on an operator split method (elastic predictor-frictional sliding corrector) is used for numerical integration of the friction constitutive equations. The simulation of a series of sliding tests is carried out and the results are compared with experiments.

---

† Present address: Technical Development Bureau, Nippon Steel Co., 20-1 Shintomi, Futtsu, Chiba-Ken, Japan 299-12.

Phil. Trans. R. Soc. Lond. A (1996) **354**, 819–843
Printed in Great Britain

1. Introduction

Over the past few years a remarkable progress has been achieved in the field of computational contact mechanics. Undoubtedly, a better mathematical understanding has been one of the key factors in the development of techniques for numerical simulation of the contact problem with friction between deformable bodies. The formulation by means of variational inequalities (Duvaut & Lions 1976; Kikuchi & Oden 1988; Oden & Martins 1985) as well as the use of return mapping algorithms (Giannakopoulos 1989; Peric & Owen 1992; Stein *et al.* 1989) and tools of mathematical programming (Feijoo & Fancello 1992) have provided efficient frameworks for the numerical treatment of such problems.

Despite such advances, most numerical applications reported in the literature are still restricted to the standard Amontons–Coulomb law of perfect friction. As pointed out by Curnier (1984), such a simplified theory can represent only a limited range of tribological situations. In part, restriction to the standard Amontons–Coulomb law may be justified by the lack of more sophisticated (and well established) phenomenological models for friction. This is in clear contrast to other areas of continuum mechanics such as elasticity and plasticity.

The friction coefficient between two metallic bodies sliding relative to one another depends on the nature and topography of the surfaces in contact as well as on environmental factors (lubrication, presence of oxide films, etc.) (Hutchings 1992). During continuous sliding, these conditions at the contact interface may be constantly changing as a consequence of complex phenomena such as the deformation of asperities, wear, internal straining, chemical reactions, etc. (Oden & Martins 1985). In experiments with iron and carbon steel specimens, Suh & Sin (1981) observed variations of friction coefficient before steady state condition of the contact interfaces was reached. They attributed this phenomenon to the evolution of the surfaces topography and consequent changes in the contributions of adhesion, plowing and asperity deformation to the coefficient of friction at the early stages of sliding. Another example of deviations from the standard Amontons–Coulomb model was observed by Hashimoto *et al.* (1990) in experiments with coated steel sheets. In situations involving high normal pressures and large sliding distances, typical in deep drawing operations, the surface coating present in these materials may be worn away exposing the bulk metal and causing a dramatic increase in the friction coefficient. In situations such as the ones described above, the evolution of surface wear is a crucial factor in the definition of the frictional behaviour and numerical predictions with reasonable accuracy may demand consideration of more realistic friction rules.

The purpose of this paper is the development of a simple phenomenological model, along with an efficient computational framework, capable of simulating the frictional behaviour of contacting bodies subjected to large sliding distances.

In order to provide a background and motivation for the model, we shall discuss in § 2 some physical aspects of wear damage in metallic surfaces undergoing large frictional sliding distances.

The phenomenological model for friction is derived in § 3. Following the ideas of Curnier (1984) and Michałowski & Mróz (1978) the model relies on the consideration of an internal variable associated with the state of the contacting surface. The hardening (or softening) character of the friction rule is defined by replacing the constant friction coefficient of the Amontons–Coulomb law by a function of the internal state variable. In addition, based on energy considerations, the internal variable is taken as

PHILOSOPHICAL TRANSACTIONS OF THE ROYAL SOCIETY A MATHEMATICAL, PHYSICAL & ENGINEERING SCIENCES

Table 1. *Friction categories – classification by Oden & Martins (1985)*

type	category	characteristic
I	quasi-static dry friction	small relative sliding
II	dynamic, sliding friction	steady state sliding
III	wear and plowing	considerable alteration of interface topography

the density of *frictional work* expended on the contact interface. The resulting theory is analogous to classical work hardening elastoplasticity. The effects of temperature, lubrication and straining of the bulk material are not taken into account.

In § 4, the technique for experimental identification of the proposed model is described for the particular case of sheet materials and the material parameters obtained for an electrogalvanized, a galvannealed and a BAF Al-killed steel sheet are presented. The identification method does not require microscopic measurements and, for sheet materials, is based on relatively simple *flat sheet sliding tests*.

A framework for the numerical simulation of the model is briefly described in § 5. It relies on a fully implicit displacement based finite-element method. The solution of the discrete incremental boundary value problem is obtained by means of the standard Newton–Raphson iterative scheme. At the local level, an algorithm based on a general operator split method is used in the numerical integration of the friction constitutive equations. The procedure, described in § 5 *a*, is a generalization of elastic predictor-plastic corrector schemes used in classical elastoplasticity. To illustrate the suitability of the numerical framework to the simulation of the proposed phenomenological model, the finite-element simulation of sliding tests is provided in § 5 *b* and the results are compared with experiments. Finally, in § 6, the conclusions of this work are presented.

2. Physical considerations and motivation

The physical mechanisms involved in the frictional contact between metallic bodies are extremely complex. Phenomena such as wear, tear, plowing, interaction between wear particles, lubricant and bulk material have a direct influence on the micromechanical properties of the contacting surfaces and, consequently, on the evolution of the frictional behaviour (Hutchings 1992; Suh & Sin 1981). Due to the complexity of the friction phenomenon, it is largely accepted that all friction effects can not be described by a single theory. Thus, any model, either phenomenological or micromechanical, must have its range of applicability limited by a set of physical conditions. Restricted to the study of contact with relative sliding between dry, metallic surfaces with engineering finishes, Oden & Martins (1985) proposed the division of frictional effects into the three general categories listed in table 1.

The effects classified as type I incorporate the friction mechanisms arising when two metallic surfaces are pressed and displaced slowly relative to one another in static equilibrium. The relative displacements are small and the frictional dissipation is dominated by the plastic deformation of asperities as well as the formation and rupture of elastoplastic junctions on the contact interface. In a large number of practical applications, such as the analysis of bolted contacting mechanical compo-

PHILOSOPHICAL TRANSACTIONS OF THE ROYAL SOCIETY A MATHEMATICAL, PHYSICAL & ENGINEERING SCIENCES

nents, the standard Amontons–Coulomb law for friction has been successfully used in the phenomenological description of this category of effects.

The second class of frictional effects (type II) refers to problems involving steady-state sliding between contacting bodies. The amount of rigid relative displacement is large but the microscopic properties of the surfaces in contact are stable with no considerable damage inflicted on the material interface. Transitional changes of the interface topography at the early stages of sliding are excluded from this category of effects. Oden & Martins (1985) studied in detail the physical aspects, continuum modelling and the numerical simulation of this important class of problems.

The effects we intend to model in this paper fall within the category of frictional phenomena classified as type III in table 1. In this case, considerable (often visible) damage is induced by frictional sliding of the contacting surfaces. The relative rigid displacements are usually large and wear, tear and plowing play an essential role in the frictional dissipation mechanism. The alteration in the micromechanical properties of the contact interface may cause large variations in the frictional forces.

A wide variety of practical engineering problems involve the occurrence of wear damage associated with frictional sliding between contacting surfaces. A situation of particular interest, which motivates the present work, is typically encountered in thin sheet metal forming processes involving surface coated steel sheets. It is frequently observed in actual forming operations that, under the same lubricant condition, sheets made of the same bulk material but with different surface coatings may produce very distinct results even when their initial friction coefficients are identical. Such discrepancy in results may be attributed to the distinct wear response of each coating which induce different variations (hardening or softening) of friction coefficient during the operation. As an illustration of the complexity of the phenomena associated with frictional wear damage, microscopic aspects of surface wear, in the particular case of coated steel sheets, are discussed in the following.

(*a*) *Example: coated steel sheets*

From a microscopic point of view, surface wear in coated steel sheets is usually characterized by the flattening of micro-asperities and scratching of the coating layer. In sheet forming operations, this phenomenon is particularly noticeable in regions subjected to high contact pressures between the tool and the workpiece. Due to the high hardness of tool materials and the relative brittleness of common surface coatings, severe damage may be induced in the coating layer during such operations. In extreme cases, the coating material may be completely worn away exposing the bulk material.

To illustrate the effects of surface wear in coated sheets, figures 2 and 3 show scanning electron microscope micrographs of the outer surface of the wall portion of a typical galvannealed steel sheet after a hat channel bending operation (schematically indicated in figure 1) under two different lubricant conditions: figure 2 corresponds to a *well lubricated condition* with teflon sheets between the blank and the tool and figure 3 depicts a *severe friction condition* with blank and tool completely degreased.

The high density of white spots, corresponding to asperities, observed in figure $2b, c$ provides evidence of the negligible surface damage induced by the forming process under a well lubricated condition. In this case, the surface coat maintained its original surface feature even though cracks were generated due to the difference in ductility between the coating material and the bulk steel. On the other hand, the grey areas (without white spots) depicted in figures $3b, c$ indicate a flattened surface which was

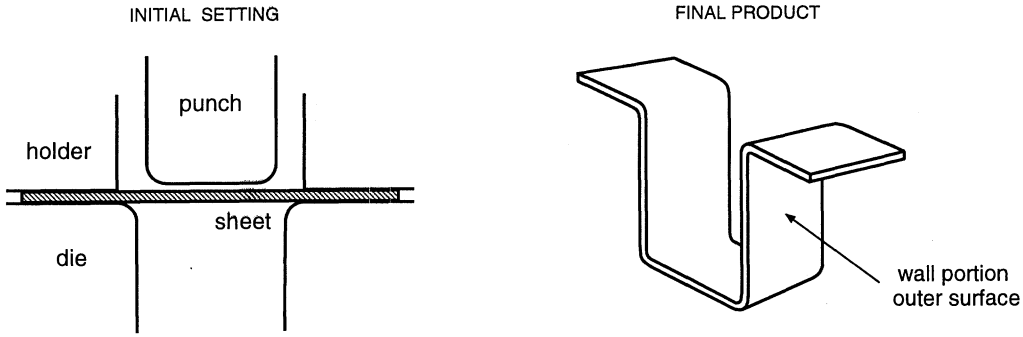

Figure 1. Hat channel bending: schematic illustration.

scoured during the forming operation under degreased conditions. Due to metal to metal contact, nearly all the contacted area of the sheet was flattened and scoured. We emphasize that the crack patterns observed in the cross section pictures (figures 2*a* and 3*a*) are very similar. Thus, the difference between the surface topography of the two sheets has been induced by frictional wear rather than by straining of the bulk material.

It is also important to note that most of the damage to the coating layer developed when the sheet surface slid against the die radius due to the high normal pressure usually present in this region. Situations like these, where surface wear is likely to occur, are frequently encountered in common sheet forming operations. Large sliding distances under high contact pressures may easily occur during the contact of the sheet with the corner regions of tools and draw beads. As we shall see in § 4, coupling between wear damage and surface phenomenological properties, such as the friction coefficient, is generally observed for metallic materials, being particularly strong for some coated steel sheets commonly used in industry. In cases such as these, the development of a phenomenological model applicable to the numerical simulation of the effects of wear damage seems to be an essential step in order to grasp finer details of the frictional behaviour not captured by the widely used Amontons–Coulomb law.

3. Phenomenological model for friction with wear effects

We develop in this section, a phenomenological model for frictional contact accounting for wear effects. The objective is to simulate the effects of surface damage in the frictional behaviour of contacting bodies subjected to large sliding distances.

(*a*) *Preliminaries*

Let us consider two bodies, one named *master* and the other *slave* body (schematically illustrated in figure 4), which may make contact with each other during their histories of deformation. The boundaries of the master and slave bodies will be denoted Γ_{m} and Γ_{s} respectively. The surface Γ_{m} is characterized by the outward unit normal field $\boldsymbol{N}$. For simplicity, we shall consider the case in which the master surface is nearly flat.

At the stage of the deformation process corresponding to the deformation mappings $\boldsymbol{\varphi}^{\mathrm{s}}$ and $\boldsymbol{\varphi}^{\mathrm{m}}$ of the slave and master bodies respectively, the *gap* separating a material point $\boldsymbol{x}$ on Γ_{s} from the master boundary Γ_{m} is defined by

$$g_{\mathrm{N}}(\boldsymbol{x}) := [\boldsymbol{\varphi}^{\mathrm{s}}(\boldsymbol{x}) - \boldsymbol{\varphi}^{\mathrm{m}}(\boldsymbol{y})] \cdot \boldsymbol{N}, \tag{3.1}$$

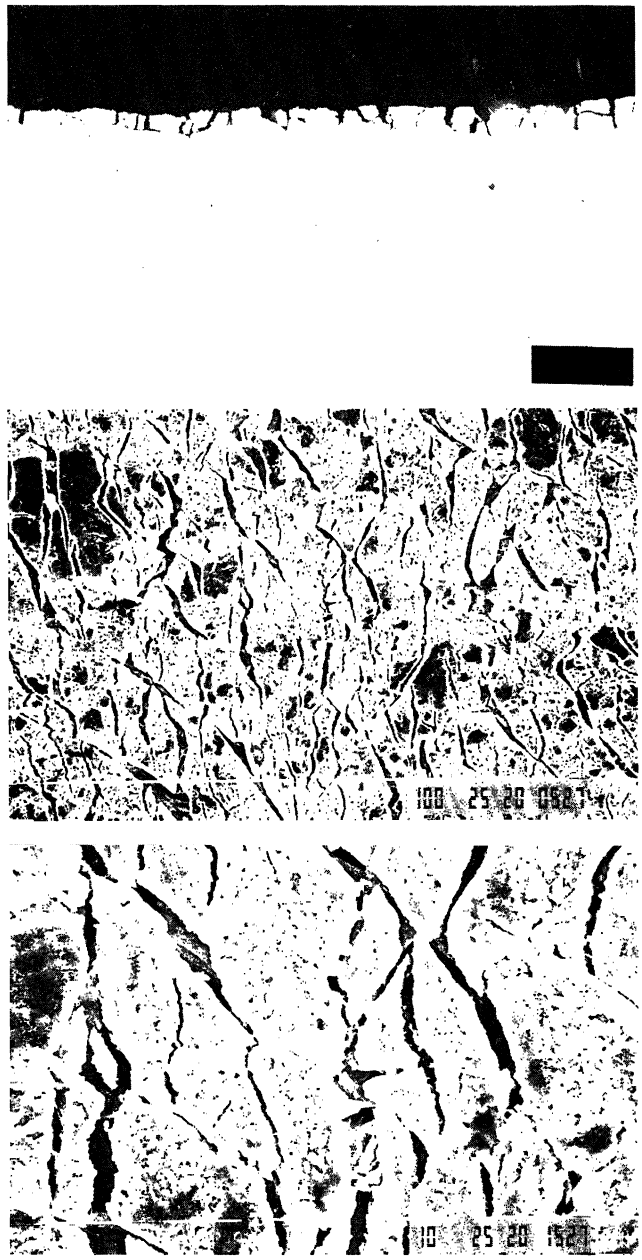

Figure 2. Galvannealed steel sheet: wall portion of hat channel product obtained under well-lubricated condition. SEM micrographs: (*a*) Cross section ×500, (*b*) outer surface ×500 and (*c*) outer surface ×1500.

where $\boldsymbol{y}$ is the material point on Γ_{s} currently defining the closest distance between $\boldsymbol{x}$ and the master body.

Let us now assume that contact has been established between $\boldsymbol{x}$ and $\boldsymbol{y}$, i.e. $g_{\mathrm{N}} = 0$. The subsequent relative displacement (under contact condition) between the two

Figure 3. Galvannealed steel sheet: wall portion of hat channel product obtained under severe friction condition (degreased). SEM micrographs: (*a*) Cross section ×500, (*b*) outer surface ×500 and (*c*) outer surface ×1500.

material points will be denoted $\boldsymbol{u}$. For convenience, it will be decomposed as

$$\boldsymbol{u} = \boldsymbol{u}_{\mathrm{T}} + u_{\mathrm{N}}\boldsymbol{N}, \tag{3.2}$$

where $\boldsymbol{u}_{\mathrm{T}} := (\boldsymbol{I} - \boldsymbol{N} \otimes \boldsymbol{N})\boldsymbol{u}$ and $u_{\mathrm{N}} := \boldsymbol{u} \cdot \boldsymbol{N}$ are, respectively, the tangential and normal components of $\boldsymbol{u}$.

PHILOSOPHICAL TRANSACTIONS OF THE ROYAL SOCIETY A MATHEMATICAL, PHYSICAL & ENGINEERING SCIENCES

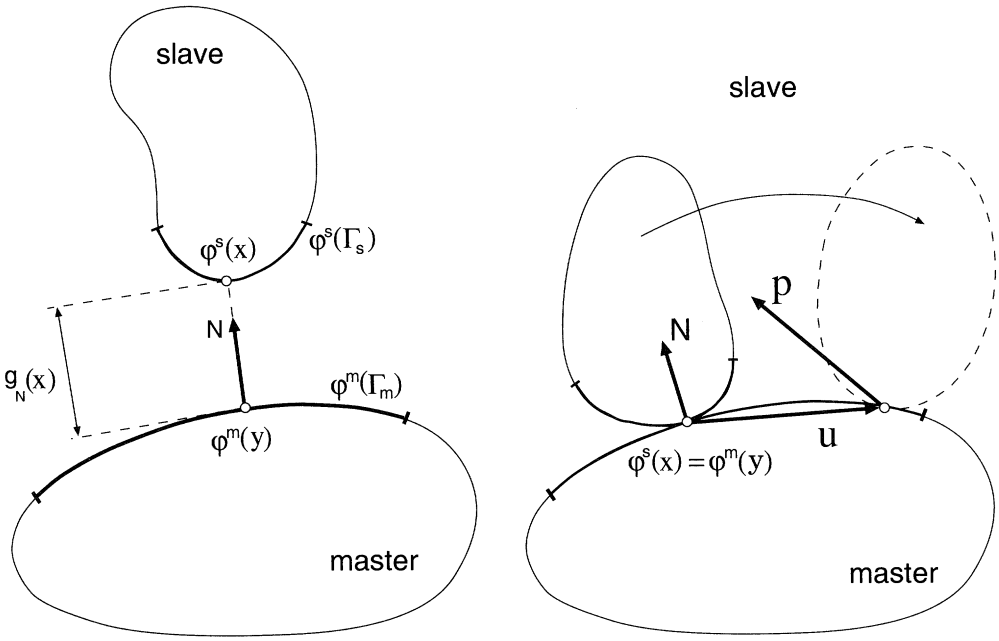

Figure 4. Contact with friction between two bodies.

The same additive decomposition will be considered for the contact pressure, $\boldsymbol{p}$, acting on the slave body, i.e.

$$\boldsymbol{p} = \boldsymbol{p}_{\mathrm{T}} + p_{\mathrm{N}}\boldsymbol{N}. \tag{3.3}$$

In the definition of the normal contact behaviour, following standard practice adopted in computational mechanics (Wriggers *et al.* 1990; Perić & Owen 1992; Feijoo & Fancello 1992), it is assumed that penetration between the two bodies is admissible. In addition, a linear relation between the normal reaction and the penetration, $g_{\mathrm{N}} < 0$, is postulated resulting in the following constitutive function for p_{N}:

$$p_{\mathrm{N}} = \begin{cases} -k_{\mathrm{N}} g_{\mathrm{N}} & \text{if} \quad g_{\mathrm{N}} < 0, \\ 0 & \text{otherwise}, \end{cases} \tag{3.4}$$

where k_{N} is the *normal stiffness* or *penalty factor*, chosen much higher than the representative stiffness of the structure, so that the geometric constraint of impenetrability is closely approximated.

In the mathematical context of convex analysis (Rockafellar 1972), the above approach represents a penalty method for solution of a constrained problem. Physically, it may be seen as a linear elastic relation between asperities deformation and normal reactions on the contacting surfaces. Within the principle of virtual work, the introduction of (3.4) in the functional of virtual work of the contact forces allows the relaxation of the impenetrability constraint ($g_{\mathrm{N}} \geqslant 0$) imposed on the set of kinematically admissible displacements. The equilibrium problem may then be approximated by use of standard finite-element techniques. Due to numerical instabilities typically associated with excessively large penalty factors, the value of k_{N} will be dictated by simultaneous consideration of accuracy and numerical stability.

(*b*) *Frictional behaviour*

Following standard arguments of the elastoplasticity theory of friction (Michałowski & Mróz 1978; Curnier 1984), we adopt the decomposition of the tangential relative velocity $\dot{\boldsymbol{u}}_{\mathrm{T}}$ into an *adherence* and a *slip* component,

$$\dot{\boldsymbol{u}}_{\mathrm{T}} = \dot{\boldsymbol{u}}_{\mathrm{T}}^{\mathrm{a}} + \dot{\boldsymbol{u}}_{\mathrm{T}}^{\mathrm{s}}, \tag{3.5}$$

along with the following constitutive law for the tangent reaction on the slave boundary,

$$\boldsymbol{p}_{\mathrm{T}} = -k_{\mathrm{T}}\boldsymbol{u}_{\mathrm{T}}^{\mathrm{a}}, \tag{3.6}$$

where k_{T} is the *tangential contact stiffness*. The evolution law for the slip component is defined by

$$\dot{\boldsymbol{u}}_{\mathrm{T}}^{\mathrm{s}} = -\dot{\gamma}\frac{\partial \Psi}{\partial \boldsymbol{p}_{\mathrm{T}}}, \tag{3.7}$$

where the *slip potential* Ψ defines the direction of frictional sliding and $\dot{\gamma}$ is consistent with the slipping/sticking condition:

$$\Phi(\boldsymbol{p}, A) \leqslant 0 \qquad \dot{\gamma} \geqslant 0 \qquad \dot{\gamma}\,\Phi(\boldsymbol{p}, A) = 0. \tag{3.8}$$

The *slip criterion* Φ above, is assumed to be a function of the contact reaction $\boldsymbol{p}$ and (possibly) a set A of internal variables taking into account the history dependence of the friction phenomenon. In the case of the standard Amontons–Coulomb law, the classical assumption

$$\Phi(\boldsymbol{p}) = ||\boldsymbol{p}_{\mathrm{T}}|| - \mu p_{\mathrm{N}} \tag{3.9}$$

implies that during frictional sliding, the intensity of frictional force $\boldsymbol{p}_{\mathrm{T}}$ is linearly proportional to the contact pressure p_{N}, i.e.

$$||\boldsymbol{p}_{\mathrm{T}}|| = \mu p_{\mathrm{N}} \tag{3.10}$$

with the (constant) proportionality factor μ known as the *friction coefficient*.

Although equations (3.5) and (3.6) may also have a physical interpretation (with $\boldsymbol{u}_{\mathrm{T}}^{\mathrm{a}}$ representing the tangential elastic deformation of asperities), we shall regard their use as a regularization of the mathematical condition of perfect adherence. We emphasize that this regularization procedure results in a set of constitutive equations for frictional sliding which have the same format as those of classical elastoplasticity (Lubliner 1990). Analogously to k_{N}, the value of the tangential stiffness k_{T} will be determined by numerical considerations rather than experimental identification.

For *isotropic* frictional contact, frictional sliding may occur only in the direction opposite to the tangential reaction. Hence, the slip potential Ψ is given by

$$\Psi(\boldsymbol{p}_{\mathrm{T}}) = ||\boldsymbol{p}_{\mathrm{T}}||. \tag{3.11}$$

(i) *Hardening: frictional wear*

As the central hypothesis of the present model for friction, we modify the slip criterion (3.9) of the classical Coulomb law and postulate,

$$\Phi(\boldsymbol{p}, w) = ||\boldsymbol{p}_{\mathrm{T}}|| - \mu(w)p_{\mathrm{N}}, \tag{3.12}$$

where *the friction coefficient, μ, is now assumed to be a function of the single scalar internal variable w* defined on the *slave* boundary. This hypothesis is based on the experimental observation of considerable changes in frictional forces as a consequence of wear in metallic surfaces. In contrast to the standard Coulomb law, it implies that

Box 1. *Constitutive model for frictional contact with hardening.*

(i) Additive decomposition of the relative tangential velocity:

$$\dot{\boldsymbol{u}}_T = \dot{\boldsymbol{u}}_T^{\mathrm{a}} + \dot{\boldsymbol{u}}_T^{\mathrm{s}}.$$

(ii) Linear elastic law for boundary reaction:

$$\boldsymbol{p}_T = -k_T \boldsymbol{u}_T^{\mathrm{a}}, \qquad p_N = -k_N g_N.$$

(iii) Slip criterion:

$$\Phi(\boldsymbol{p}, w) = ||\boldsymbol{p}_T|| - \mu(w) p_N.$$

(iv) Slip potential and slip rule:

$$\Psi(\boldsymbol{p}) = ||\boldsymbol{p}_T||, \quad \dot{\boldsymbol{u}}_T^{\mathrm{s}} = -\dot{\gamma}\boldsymbol{T}, \quad \boldsymbol{T} = \frac{\partial \Psi}{\partial \boldsymbol{p}} = \frac{\boldsymbol{p}_T}{||\boldsymbol{p}_T||}.$$

(v) Evolution law for the internal variable w:

$$\dot{w} = -\boldsymbol{p}_T \cdot \dot{\boldsymbol{u}}_T^{\mathrm{s}} = \dot{\gamma}\, ||\boldsymbol{p}_T||.$$

(vi) Slipping/sticking condition:

$$\Phi \leqslant 0, \qquad \dot{\gamma} \geqslant 0, \qquad \dot{\gamma}\Phi = 0.$$

during frictional sliding, the tangential reaction is a function of the normal pressure *and* the thermodynamical variable w related to the state of surface wear,

$$||\boldsymbol{p}_{\mathrm{T}}|| = \mu(w) p_{\mathrm{N}}, \tag{3.13}$$

i.e. under constant normal pressure, the frictional force may *harden* or *soften* according to the evolution of w.

To completely define the model, an evolution law for the internal state variable w is required. Here, we shall take w as the density of *frictional work* expended on the surface point considered. Hence, its evolution equation is defined by

$$\dot{w} = -\boldsymbol{p}_{\mathrm{T}} \cdot \dot{\boldsymbol{u}}_{\mathrm{T}}^{\mathrm{s}}, \tag{3.14}$$

and the resulting constitutive model for frictional contact with hardening is analogous to classical work hardening plasticity. For convenience it is summarized in box 1. The reason for this choice of w is simple: we have assumed that the amount of energy dissipated by the frictional process is directly connected to the alteration of the micromechanical constitution of the material interface†. Such changes in surface topography are phenomenologically reflected in the variation of the friction coefficient. Note that with such a choice for w, the effects of temperature, lubrication and internal straining on the coefficient of friction have *not* been taken into account in the present theory.

Remark 3.1. Independently of the particular choice for w, the function $\mu : \mathcal{R} \rightarrow$

† Based on a similar argument, Rigney & Hirth (1979) predicted the steady-state friction coefficient of metals by equating the frictional work to the energy required to deform plastically the near surface region. More recently, Qiu & Plesha (1991) proposed a theory for steady-state frictional wear which relates the wear rate to the frictional power and recovers Archard's wear model (Hutchings 1992) under certain conditions.

$\mathcal{R}^+$ in (3.12) defines the hardening (or softening) character of the frictional sliding rule. Borrowing standard terminology of classical elastoplasticity, $\mu(w)$ will be called the *frictional hardening curve. The experimental identification of this function completely characterizes the present constitutive model for friction.* It is worth noting that since the present theory was derived on a purely phenomenological basis, the measurement of microscopic properties is not required in the determination of the material parameters.

Remark 3.2. It is important to note that the variable w was defined for points of the *slave* boundary only. Consequently, the state of the master surface was assumed to have no influence on the friction coefficient between the two bodies. In other words, this assumption implies that only one of the surfaces in contact (the slave surface) is subjected to frictional wear. This hypothesis is physically reasonable in a large variety of practical engineering problems such as typical metal forming processes in which, due to its extreme hardness, the tool (master) surface does not show considerable alteration of microscopic properties while the workpiece (slave) surface may be severely damaged in one single operation. An extension of the present model to account for wear in *both* surfaces can be derived in a straightforward manner. Indeed, this could be accomplished by a simple redefinition of the friction coefficient as a function, $\mu = \mu(w_{\mathrm{m}}, w_{\mathrm{s}})$, of the densities of frictional work on the master as well as on the slave surface. However, from the experimental point of view, considerable complexity would be introduced by this assumption. In such a case, the identification of the function $\mu = \mu(w_{\mathrm{m}}, w_{\mathrm{s}})$, represented as a *surface* in $\mathcal{R}^3$, would involve the determination of the coefficient of friction for different combinations of wear states of both surfaces.

4. Experimental identification

The above general theory for friction is applied in this section to model the behaviour of some steel sheets normally used in thin sheet forming processes. This is motivated by the importance, pointed out in § 2, of the phenomenon of frictional wear in such operations. The technique for experimental identification of the frictional hardening curves is, thus, described for the particular case of sheet materials and applied to two zinc coated sheet metals: an electrogalvanized (EG) and a galvannealed steel sheet (GA), as well as to a cold rolled material (*without* coating): BAF Al-killed steel sheet (CR). We remark that, since the factors considered in the derivation of the present theory are independent of the geometry of the bulk material, the experimental procedure for materials other than sheets is completely analogous. The mechanical properties of the specimens used in the identification are shown in table 2 where the columns YP, TS and El correspond, respectively, to the yield stress, maximum tensile strength and elongation at rupture. The headings $\bar{n}$ and $\bar{r}$ stand respectively for the exponent of the power law hardening for plasticity and the normal anisotropy factor and R_a is the average roughness of the virgin surface.

(*a*) *The method*

For sheet materials, the identification technique is based on *flat sheet sliding tests.* The equipment used is shown in figure 5. Its components and the method used are schematically illustrated in figure 6. After degreasing, the sheet to be tested is lubri-

PHILOSOPHICAL TRANSACTIONS OF THE ROYAL SOCIETY A MATHEMATICAL, PHYSICAL & ENGINEERING SCIENCES

Table 2. *Steel sheets – mechanical properties*

mat.	coat weight (g m^{-2})	YP (N mm^{-2})	TS (N mm^{-2})	El (%)	$\bar{n}$ 5–15%	$\bar{r}$ 15%	R_a (μm)	hardness (Hv 10g)
EG	20/20	169.2	310.0	45.4	0.243	1.60	0.81	82
GA	60/60	199.1	319.3	42.7	0.216	1.64	1.06	208
CR	—	168.5	317.7	43.3	0.240	1.56	0.72	142

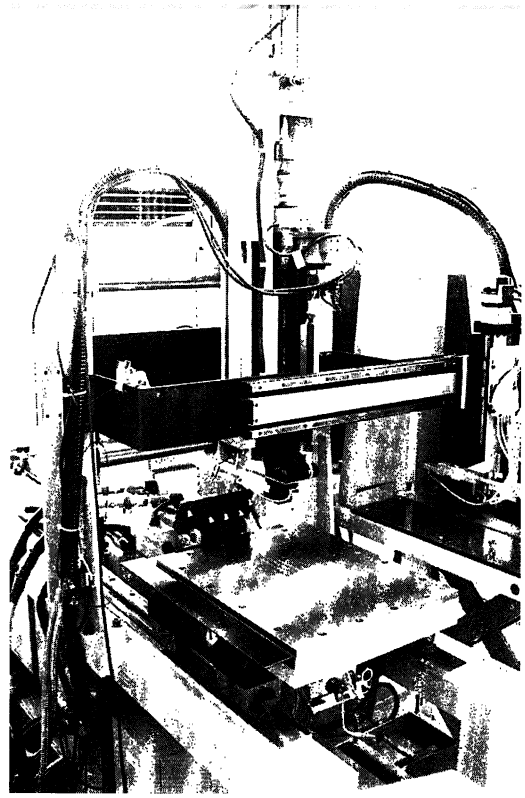

Figure 5. Flat sheet sliding machine.

cated with washing oil (with kinematic viscosity 2.9*cSt* at 40 °C) and clamped to the sliding table (note that coated sheets are normally stamped under this poor lubrication condition). A prescribed normal force, F_N, is then applied to the tip of the tool material (SKD-11) whose geometry is shown in figure 6. The tip is kept fixed during the experiment and to avoid rotation and ensure high precision in the determination of the friction coefficient, it is anchored to a sufficiently rigid structure. Once the normal force has been applied, the table slides 300 mm, driven by a hydraulic cylinder as represented in figure 6. After sliding, the normal force is released and the table returns to its initial position. The normal force is then reapplied and the cycle is repeated several times.

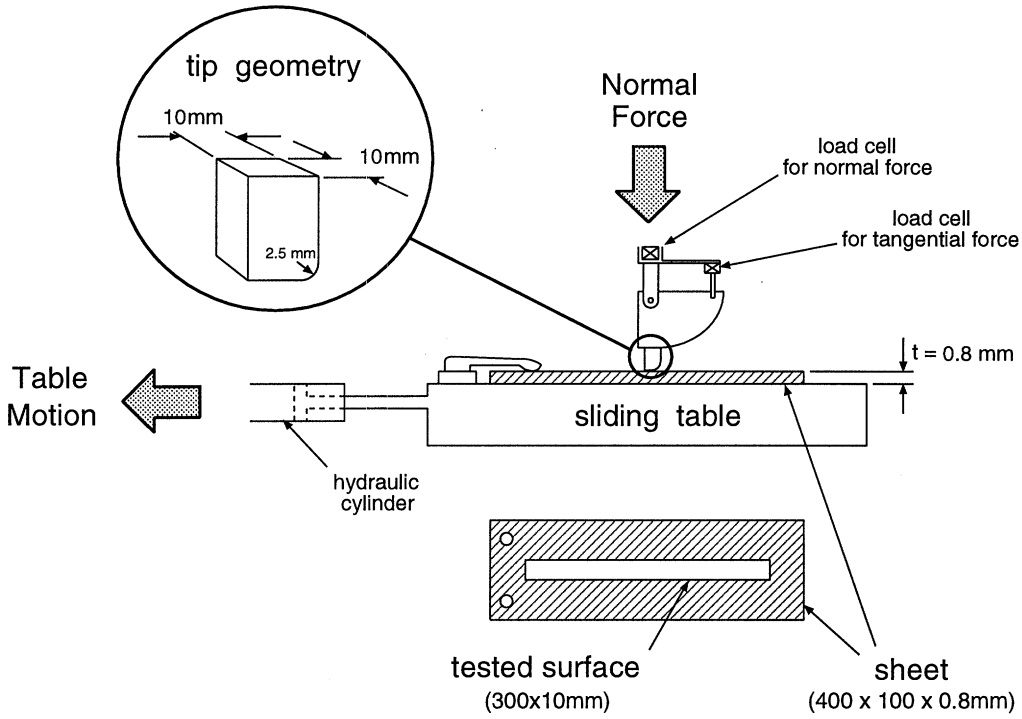

Figure 6. Experimental identification: sliding test.

Table 3. *Frictional hardening curves – polynomial coefficients* ($\mu(w) = \alpha_0 + \alpha_1 \times w + \alpha_2 \times w^2 + \ldots$; w measured in kN cm^{-1}.)

mat.	α_0	α_1	α_2	α_3	α_4	α_5
EG	0.157	-0.315×10^{-1}	0.104×10^{-1}	-0.821×10^{-3}	0.289×10^{-4}	-0.410×10^{-6}
GA	0.178	-0.666×10^{-2}	—	—	—	—
CR	0.145	-0.876×10^{-2}	—	—	—	—

During each sliding, the friction coefficient μ is determined by

$$\mu = F_{\mathrm{T}}/F_{\mathrm{N}}, \tag{4.1}$$

where F_{T} is the average tangential force measured by the load cell indicated in figure 6. The corresponding density of frictional work expended at points of the *sheet* surface is computed by simply integrating the average tangential pressure over the sliding distance (the sliding distance in this case is the length of the tip in contact with the specimen – approximately 7.5 mm) generating a set of points (μ, w) which define a frictional hardening curve for the prescribed intensity of normal force.

This operation is carried out at various levels of normal force within the range of the machine capacity (0.49–3.92 kN) and the final frictional hardening function is obtained as a least squares polynomial fit of the experimental points obtained at each level. Obviously, for a material which is adequately described by the present model, i.e. for a material whose friction coefficient depends on w, a single curve must

(a)

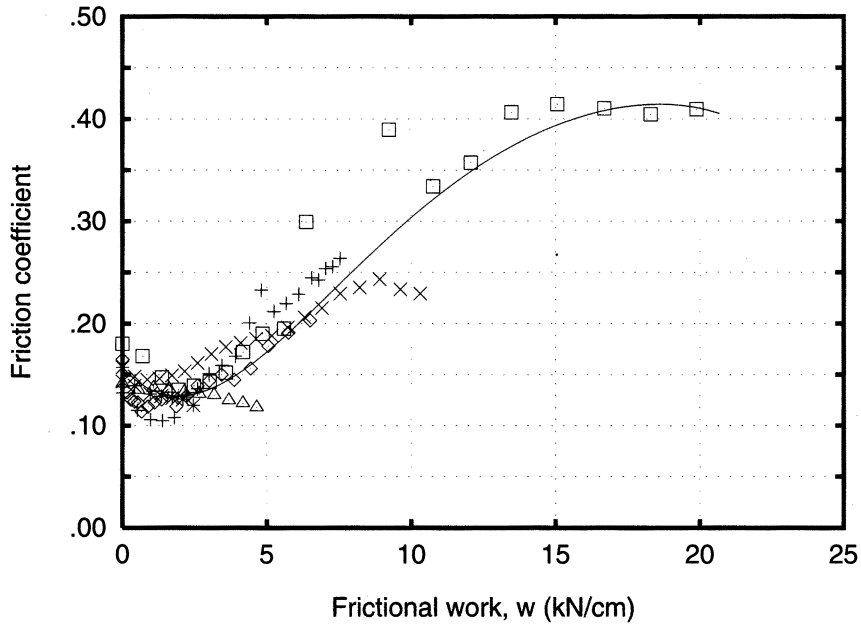

(b)

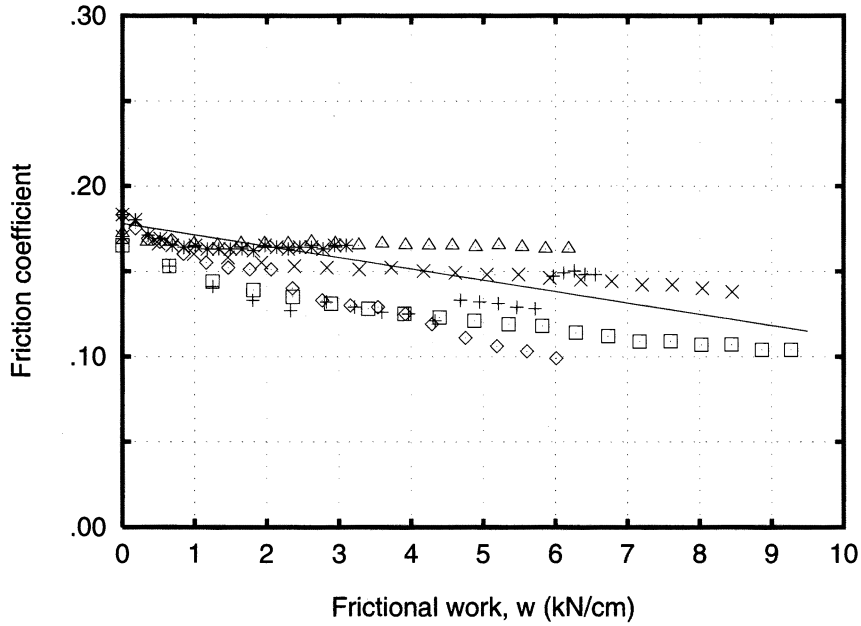

Figure 7. Frictional hardening curves. Experimental determination. (*a*) Electrogalvanized steel sheet – EG; (*b*) galvannealed steel sheet – GA.

be able to fit satisfactorily the points obtained at different normal loads. In case the experimental points can not be reasonably fitted with a single curve, a more complex

PHILOSOPHICAL TRANSACTIONS OF THE ROYAL SOCIETY A MATHEMATICAL, PHYSICAL & ENGINEERING SCIENCES

(*c*)

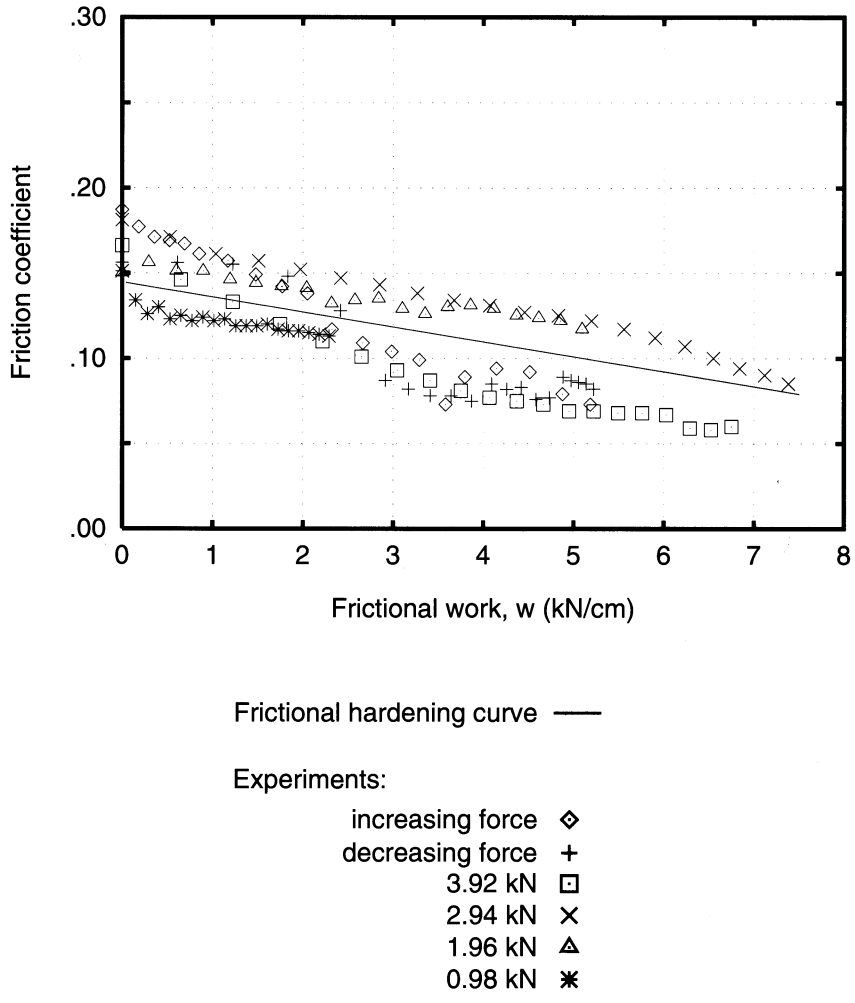

Figure 7. Frictional hardening curves. Experimental determination. (*c*) BAF Al-killed steel sheet – CR.

model, involving additional internal variables, would be required for an appropriate description of the frictional behaviour.

(*b*) *Results*

Following the procedure described above, the frictional hardening curves for electrogalvanized (EG), galvannealed (GA) and BAF Al-killed steel sheets (CR) were determined. The coefficients of the polynomial functions

$$\mu(w) = \alpha_0 + \alpha_1 \times w + \alpha_2 \times w^2 + \ldots \tag{4.2}$$

obtained for each material are shown in table 3. The corresponding curves, along with the experimental points obtained, are plotted in figure 7.

The experimental points used to determine the hardening curves were obtained

with four different levels of *constant* normal force (always starting with a virgin specimen): $F_N = 0.98$ kN, $F_N = 1.96$ kN, $F_N = 2.94$ kN and $F_N = 3.92$ kN. Points obtained following more complex load paths, in which the normal force is variable, are also plotted in figure 7. In this case, two particular paths have been considered: *increasing* and *decreasing* normal pressure. For increasing normal load, starting with a virgin sheet, a sequence of four sets of five sliding cycles each is executed, respectively, with $F_N = 0.98$ kN, $F_N = 1.96$ kN, $F_N = 2.94$ kN and $F_N = 3.92kN$ (in this order). The procedure for decreasing normal load is the same except for the order of the forces which is reversed, i.e. it is started with $F_N = 3.92$ kN and, in the last five passes $F_N = 0.98$ kN.

Figure 7*a* shows the results obtained for the electrogalvanized steel sheet tested. Generally, an initial softening due to flattening of micro-asperities is followed by a substantial increase in friction coefficient. The friction coefficient ranges between 0.13 and 0.41 approximately. This phenomenon may be attributed to the removal of its relatively soft zinc coat layer and the subsequent interaction between the bulk material and wear particles. This process seems to be attenuated by the presence of a harder surface coating in the galvannealed sheet. In contrast with the behaviour of the electrogalvanized sheet, figures 7*b* shows the progressive softening experienced by the GA sheet tested. The same softening tendency is observed for the cold rolled sheet (figure 7*c*). For both materials, data obtained at different levels of normal pressure were well approximated by a linear function. For CR, the absence of surface coating makes the variation of the frictional behaviour to be dominated by the plastic deformation of asperities. With increasing sliding distance, the asperities become flatter reducing the deformation contribution to the friction coefficient. It should be observed that, for the three materials considered, the frictional hardening curve obtained fits well all experimental data, including the points obtained with the *variable load* paths. This clearly demonstrates the suitability of the density of frictional work as a history recording parameter for the phenomenon of frictional wear.

5. Numerical simulation

To illustrate the suitability of the present theory to the simulation of effects of surface wear damage in large scale problems, a framework for the computational treatment of the proposed phenomenological model for friction is described in this section. Some numerical examples, involving the sliding tests presented above, are provided.

The strategy for the numerical simulation of the model relies on a fully implicit displacement based finite-element method. As a result of the basic constitutive hypothesis (3.4), the penalty method is used in the enforcement of the impenetrability constraint. The contact condition is monitored by checking penetration of the slave nodes on master surfaces as described by Perić & Owen (1992). In contrast to the practice of considering nodal *forces* as the outcome of the normal contact constitutive equation, common in most of the current computational contact mechanics literature, the approach adopted in this work relates *pressures* to normal penetration as in the original constitutive law (3.4). Since the present theory relies on the *density* of frictional work (pressure integrated over sliding distance) as an internal variable, the use of forces in the friction constitutive equations would lead to physically meaningless results. The standard Newton–Raphson scheme, arising from the exact linearization of the principle of virtual work, is used in the solution of the

Box 2. *Numerical integration algorithm for frictional contact with hardening*

(i) Given incremental displacement, $\Delta \boldsymbol{u}$, update configuration and normal reaction

$$\boldsymbol{\varphi}_{n+1} = \boldsymbol{\varphi}_n + \Delta \boldsymbol{u}, \quad p_{Nn+1} = p_{Nn} - k_N \Delta u_N.$$

(ii) Elastic predictor

Evaluate *elastic trial* frictional force

$$\boldsymbol{p}_{Tn+1}^{\text{trial}} = \boldsymbol{p}_{Tn} - k_T \Delta \boldsymbol{u}_T.$$

Check slip condition

$$\text{IF} \quad \Phi = ||\boldsymbol{p}_{Tn+1}^{\text{trial}}|| - \mu(w_n) p_{Nn+1} \leqslant 0,$$

$$\text{THEN set} \quad (\cdot)_{n+1} = (\cdot)_{n+1}^{\text{trial}} \quad \text{and EXIT.}$$

(iii) Frictional slip corrector

Solve the system for $\Delta\gamma$ and w_{n+1}

$$||\boldsymbol{p}_{Tn+1}^{\text{trial}}|| - k_T \Delta\gamma - \mu(w_{n+1}) p_{Nn+1} = 0,$$

$$w_{n+1} - w_n - \mu(w_{n+1}) p_{Nn+1} \Delta\gamma = 0.$$

Update frictional force

$$\boldsymbol{p}_{Tn+1} = \mu(w_{n+1}) p_{Nn+1} \boldsymbol{T}_{n+1},$$

$$\text{with} \quad \boldsymbol{T}_{n+1} = \boldsymbol{p}_{Tn+1}^{\text{trial}} / ||\boldsymbol{p}_{Tn+1}^{\text{trial}}||.$$

discrete incremental boundary value problem. The algorithm used at the nodal level, for the integration of the proposed frictional contact constitutive equations, is briefly described below.

(*a*) *Integration algorithm*

The similarity between rate independent elastoplasticity and the regularized contact problem with friction makes numerical techniques used in classical elastoplasticity particularly suitable for integration of the constitutive equations presented in § 3.

In the present work, we shall use an algorithm based on general *operator split methodology* for the numerical integration of the equations of frictional contact with hardening. The method relies on the sequential application of two procedures: an *elastic predictor*, where only the elastic relations are considered, followed by a *frictional slip corrector* in which the rate evolution equations are solved taking the result of the predictor stage as initial condition†. In the corrector stage the rate equations of box 1 are approximated by a one step *backward* Euler scheme. The resulting system of nonlinear algebraic equations is solved by the standard Newton–Raphson method. The algorithm is conveniently summarized in box 2 where we consider the integration over a typical time interval $[t_n, t_{n+1}]$.

† Predictor–corrector algorithms have been extensively used in computational plasticity (Mitchell & Owen 1988; Perić *et al.* 1992*a*; Simo & Hughes 1987). We refer to Perić & Owen (1992) for a recent application in the context of the standard Amontons–Coulomb law for friction.

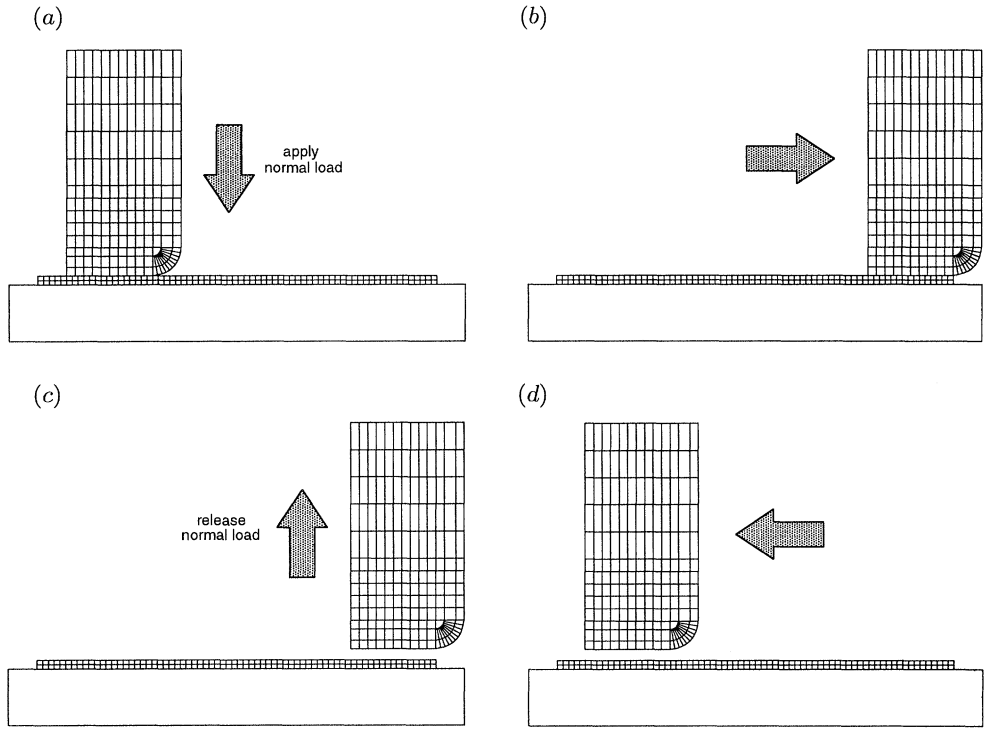

Figure 8. Finite-element meshes: sliding cycle. (*a*) Initial configuration; (*b*) sliding; (*c*) release normal force, and (*d*) return to initial configuration. The arrows indicate the relative motion between the tip and the table.

(*b*) *Simulation of sliding tests*

As pointed out in the introductory section of this paper, the primary objective of the developments presented above is to provide a framework for the efficient simulation of effects of frictional wear in the solution of practical engineering problems. In order to achieve the necessary efficiency, the constitutive theory must closely represent the physical phenomenon and, at the same time, the numerical scheme, comprising the integration algorithm and the finite-element structure, must be able to emulate the constitutive model to the desired degree of accuracy in a sufficiently wide range of circumstances.

It has already been established in § 4 that the present phenomenological theory can correctly represent the effects of frictional wear. To show the suitability of the adopted numerical framework to the simulation of frictional contact with wear in large scale problems, the sliding tests reported in § 4 are numerically simulated in this section. It should be pointed out that, in spite of the relative simplicity of such tests, they contain the basic ingredients typical of practical problems of interest: contact between two or more bodies with very large relative displacements. The simulation is carried out here for the electrogalvanized, the galvannealed and the BAF Al-killed steel sheets and the geometry of the problem as well as the experimentally determined hardening curves correspond to those described in § 4. For each material, the simulation is carried out for the two types of load path discussed: constant and variable normal force.

A mesh containing 180 four-noded quadrilateral elements (plane strain state is assumed) is used in the discretization of the tip. The sheet is discretized by two layers with 60 elements each and the nodes on its left edge are constrained. The sliding table is considered rigid and is represented by one single element. The finite-element mesh is shown in figure 8. For simplicity, only 30 mm of the sheet length has been considered in the finite-element simulation.

At the beginning of a sliding cycle, the tip lies at 5 mm from the left edge of the sheet (see figure 8*a*). Starting from this initial configuration and after the normal force is applied, a relative sliding $d = 25$ mm between the table and the tip is incrementally imposed. This ensures an approximately 10 mm long evenly worn region on the sheet surface (between 7.5 mm and 17.5 mm from the left edge). When d reaches 25 mm (figure 8*b*) the normal force is released, the tip is lifted (figure 8*c*) and returned to its initial position (figure 8*d*) thereby closing a cycle. Note that a 'steady state' frictional force will occur when the entire surface of the tip contacts the evenly worn region of the sheet. This corresponds to relative sliding between 7.5 and 10 mm (in the experimental procedure of § 4 this region is much longer but this difference is immaterial for the present purpose). We remark that, in the determination of the material parameters, the contact pressure along the face of the tip was taken as a constant (average) value and the frictional hardening curve was obtained in an averaged sense. In the finite-element simulation, the variations of normal pressure are accounted for with the friction hardening law being valid pointwise.

(i) *Electrogalvanized steel sheet*

The tangential reaction force on the tip obtained in the numerical simulation of the sliding tests with electrogalvanized steel sheet are plotted in figures 9 and 10 for each cycle. The results obtained experimentally are also plotted for comparison. Figure 9 corresponds to the tests performed at constant normal loads and figure 10 shows the results for variable forces.

The good agreement between the simulation and experiments, depicted in figure 9, confirms the accuracy of the adopted numerical framework. At high normal pressures (figures 9*a*, *b*), substantial hardening is detected in the tests. With 3.92 kN prescribed normal force, the tangential reaction on the tip ranges approximately between 0.5 kN in the 5th pass and 1.6 kN in the 20th pass. Obviously, in this case, the use of the standard Amontons–Coulomb law of friction would lead to unacceptably inaccurate numerical predictions. With lower normal pressure ($F_{\mathrm{N}} = 0.98$ kN), a slight softening is detected during the cycles.

Since the sliding distance is proportional to the number of passes and does not depend on the normal pressure, the use of a similar model expressed in terms of sliding distance (i.e. replacing w by the sliding distance in the present theory) would also result in erroneous predictions. Such a model would not be able to reproduce softening followed by hardening at high pressures and also represent only softening at lower pressures. Note that if the friction coefficient were plotted against the sliding distance in figure 7*a*, the corresponding experimental points could not be fitted with a single hardening curve.

In the tests with variable normal force (figure 10) a remarkable correspondence between numerical simulation and experiments is also observed. This is an obvious consequence of the proximity between the experimental points for variable force and the fitting hardening curve observed in figure 7*a*. Again, we remark that the

PHILOSOPHICAL TRANSACTIONS OF THE ROYAL SOCIETY A MATHEMATICAL, PHYSICAL & ENGINEERING SCIENCES

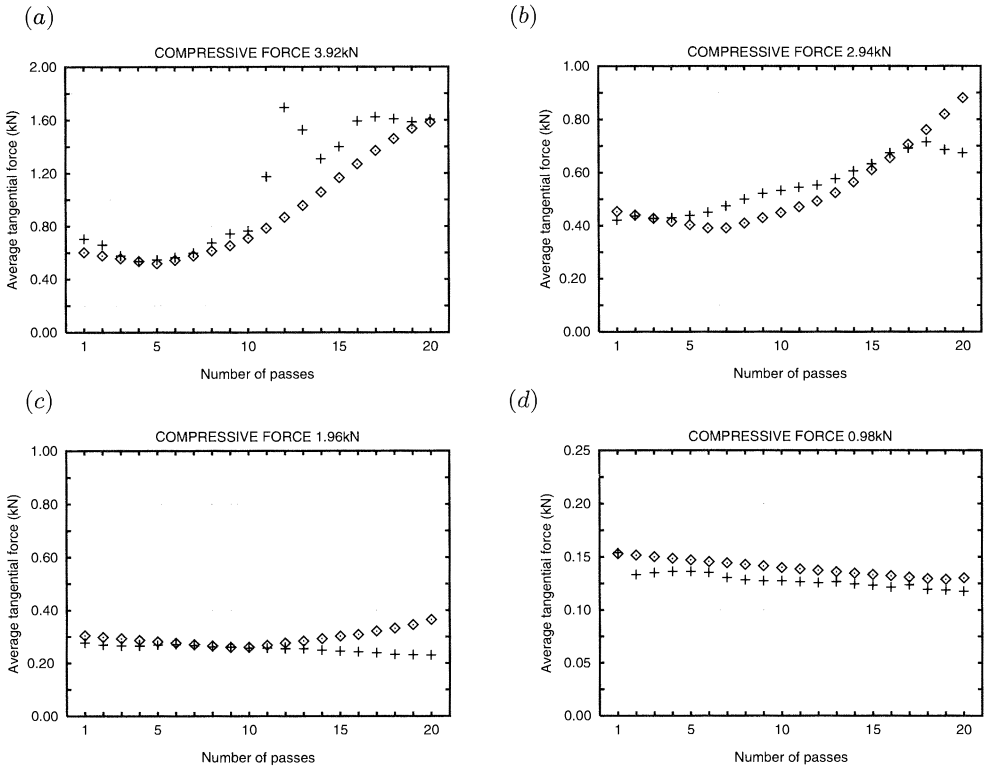

Figure 9. Sliding tests with EG steel sheet at constant normal forces. ◇, FE simulation; +, experiment. (*a*) Normal force = 3.92 kN; (*b*) normal force = 2.94 kN; (*c*) normal force = 1.96 kN; (*d*) normal force = 0.98 kN.

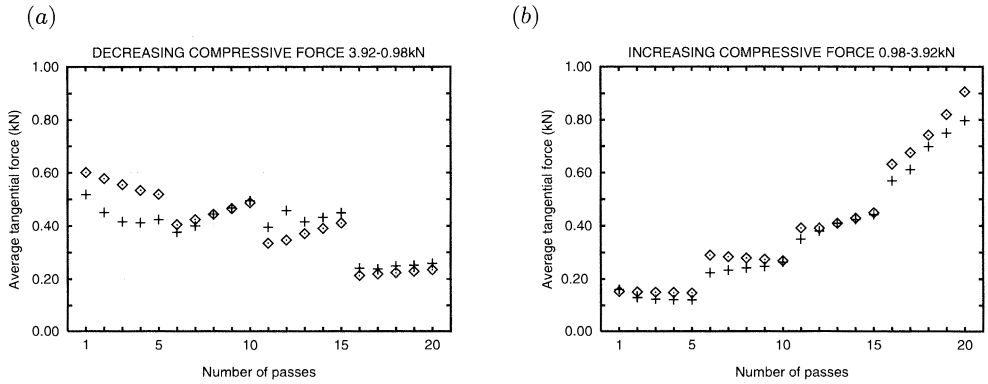

Figure 10. Sliding tests with EG steel sheet for variable normal forces. ◇, FE simulation; +, experiment. (*a*) Decreasing normal force: passes [1–5] → $F_N = 3.92$ kN, passes [6–10] → $F_N = 2.94$ kN, passes [11–15] → $F_N = 1.96$ kN, passes [16–20] → $F_N = 0.98$ kN. (*b*) Increasing normal force: passes [1–5] → $F_N = 0.98$ kN, passes [6–10] → $F_N = 1.96$ kN, passes [11–15] → $F_N = 2.94$ kN, passes [16–20] → $F_N = 3.92$ kN.

agreement in such complex loading paths supports the use of the density of frictional work as the internal variable associated with variations of the friction coefficient.

To illustrate the complexity of the boundary value problem solved, figure 11 shows the Von Mises equivalent stress distribution on the sheet and tip at the initial stage

PHILOSOPHICAL TRANSACTIONS OF THE ROYAL SOCIETY A MATHEMATICAL, PHYSICAL & ENGINEERING SCIENCES

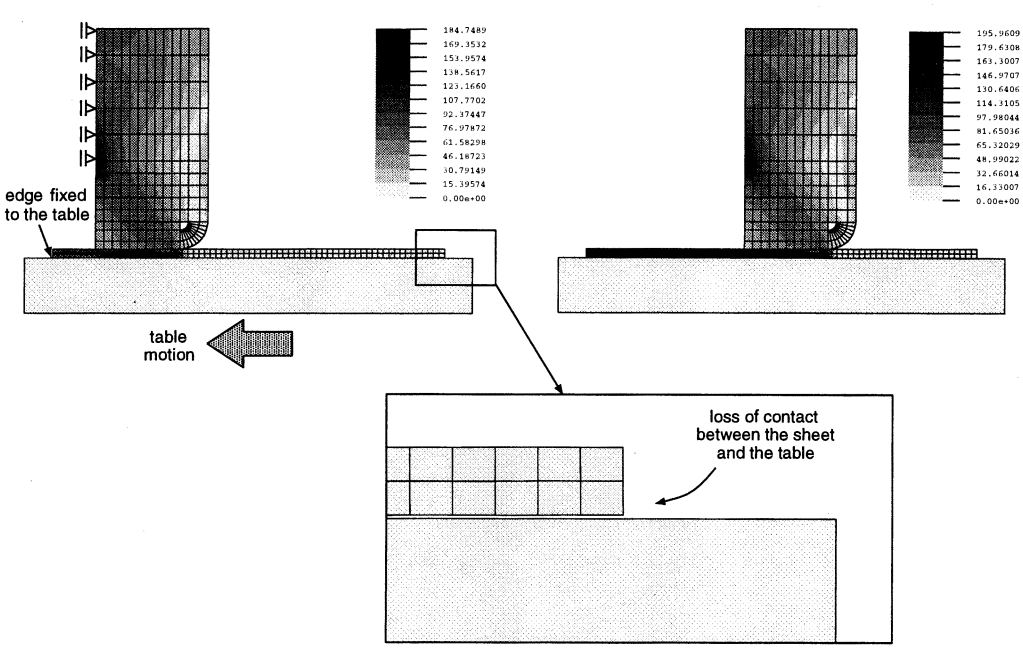

Figure 11. Von Mises effective stress distribution (N mm^{-2}). EG at constant 3.92 kN normal load – 20th pass.

of sliding as well as during 'steady' sliding (the entire tip surface contacting the evenly worn region of the sheet). The results shown correspond to the 20th pass of the simulation with constant 3.92 kN normal load. We point out the loss of contact between the right edge of the sheet and the table occurring at the beginning of the sliding cycle.

(ii) *Galvannealed steel sheet*

In figures 12 and 13 we present the results for the galvannealed steel sheet. As expected from the closeness between the fitting hardening curve and the experimental points observed in figure 7*b*, all results agree well with the experiments.

(iii) *BAF Al-killed steel sheet*

Figures 14 and 15 show the results for BAF Al-killed steel sheet. In all cases, the adopted numerical scheme reproduces the good agreement between theory and experiments observed in figure 7*c*. With high constant normal forces (figure 14), a considerable softening is observed while at low pressure (2.94 kN) only a small amount of softening occurs. This reinforces the adequacy of the present constitutive-numerical framework for the simulation of the frictional behaviour of this cold rolled material.

6. Concluding remarks

A phenomenological model for frictional contact accounting for wear effects was proposed. By adopting the frictional work as the internal variable associated to the state of the contacting surfaces, a theory analogous to classical work hardening elastoplasticity was obtained. The model is simple and its incorporation into existing

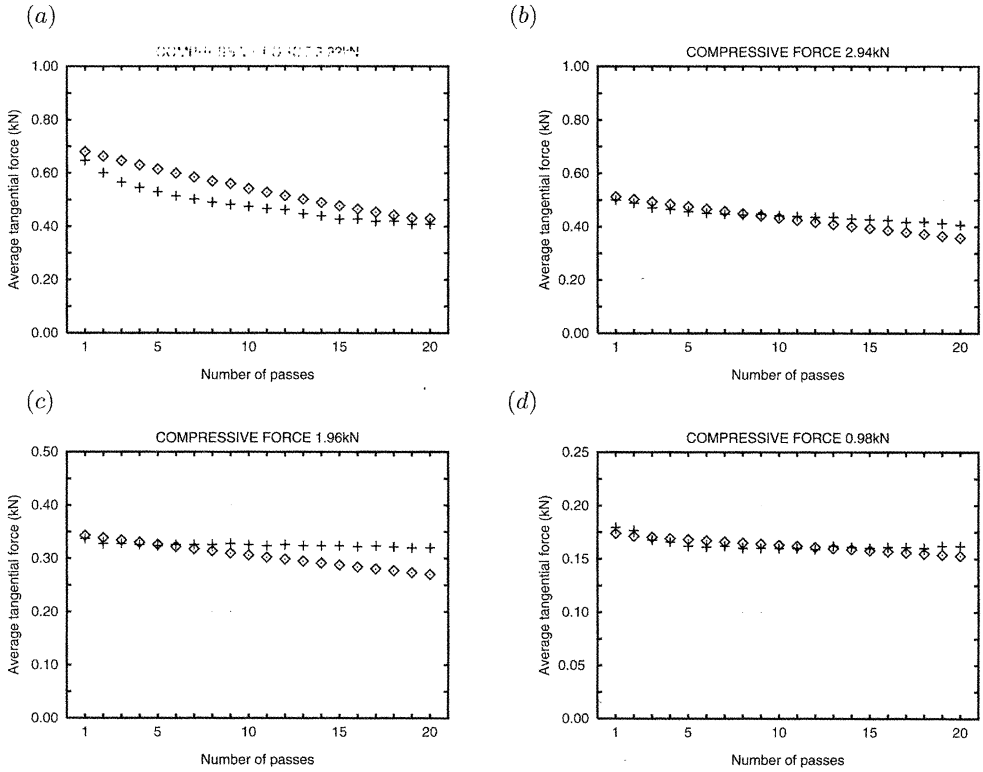

Figure 12. Sliding tests with GA steel sheet at constant normal forces. ◇, FE simulation; +, experiment. (*a*) Normal force = 3.92 kN; (*b*) normal force = 2.94 kN; (*c*) normal force = 1.96 kN; (*d*) normal force = 0.98 kN.

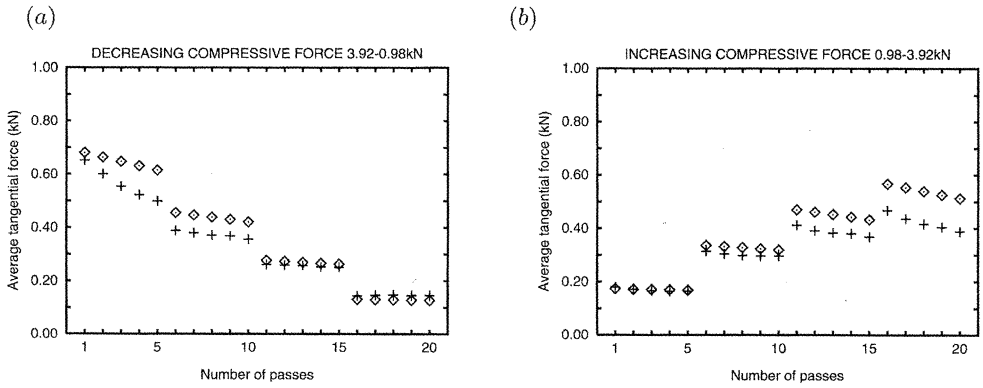

Figure 13. Sliding tests with GA steel sheet for variable normal forces. ◇, FE simulation; +, experiment. (*a*) Decreasing normal force: passes [1–5] → F_N = 3.92 kN, passes [6–10] → F_N = 2.94 kN, passes [11–15] → F_N = 1.96 kN, passes [16–20] → F_N = 0.98 kN. (*b*) Increasing normal force: passes [1–5] → F_N=0.98 kN, passes [6–10] → F_N = 1.96 kN, passes [11–15] → F_N = 2.94 kN, passes [16–20] → F_N = 3.92 kN.

finite-element codes for computer simulation of large scale engineering problems is relatively straightforward.

The technique for experimental identification of the material parameters was described for the case of sheet materials and the frictional hardening curves for an

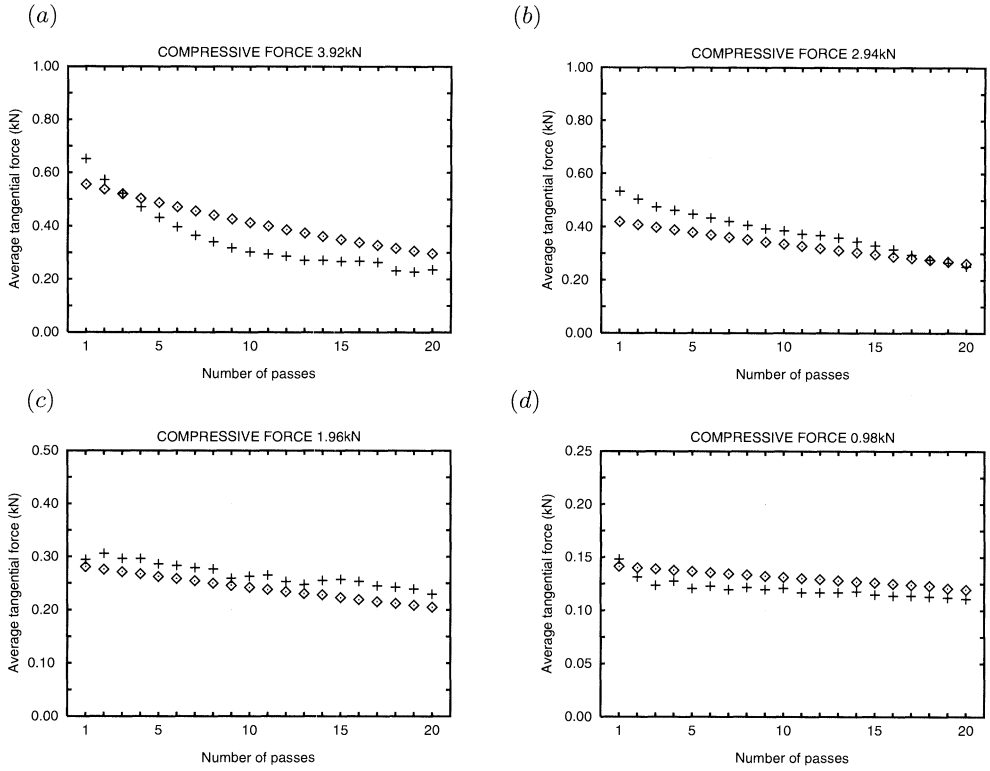

Figure 14. Sliding tests with CR steel sheet at constant normal forces. ◇, FE simulation; +, experiment. (*a*) Normal force = 3.92 kN; (*b*) normal force = 2.94 kN; (*c*) normal force = 1.96 kN; (*d*) normal force = 0.98 kN.

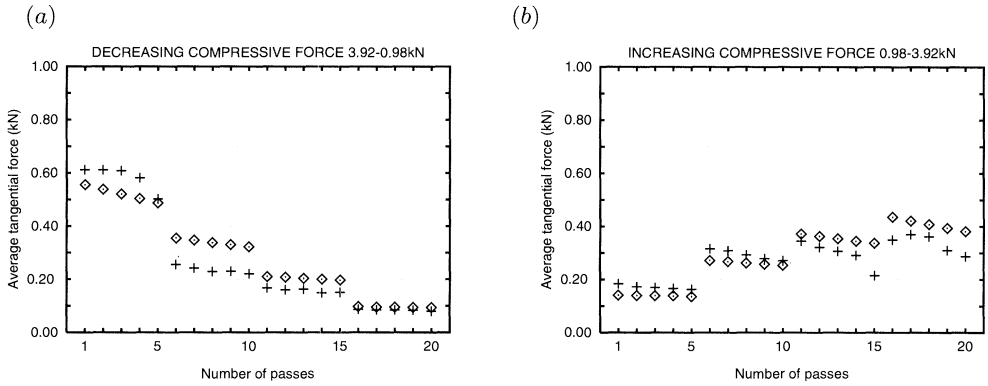

Figure 15. Sliding tests with CR steel sheet for variable normal forces. ◇, FE simulation; +, experiment. (*a*) Decreasing normal force: passes [1–5] → $F_N = 3.92$ kN, passes [6–10] → $F_N = 2.94$ kN, passes [11–15] → $F_N = 1.96$ kN, passes [16–20] → $F_N = 0.98$ kN. (*b*) Increasing normal force: passes [1–5] → $F_N = 0.98$ kN, passes [6–10] → $F_N = 1.96$ kN, passes [11–15] → $F_N = 2.94$ kN, passes [16–20] → $F_N = 3.92$ kN.

electrogalvanized, a galvannealed and a BAF Al-killed steel sheet were determined. The identification technique does not involve the measurement of microscopic properties requiring only the determination of the function $\mu = \mu(w)$. For sheet materials it is based on flat sheet sliding tests. The experimental results for the three mate-

rials considered demonstrated the adequacy of the density of frictional work as the internal variable associated with the phenomenon of frictional wear.

Based on a fully implicit displacement based finite-element scheme in conjunction with the standard Newton–Raphson procedure, a framework for the computational treatment of the proposed model was described. In this context, a robust algorithm based on operator split methodology (elastic predictor-frictional sliding corrector) was used in the local integration of the frictional constitutive equations.

The finite-element simulation of a series of sliding tests was carried out using the hardening curves determined experimentally. The results were compared with the corresponding experiments and showed the suitability of the adopted numerical framework to the simulation of the proposed model.

In summary, by exploiting concepts of phenomenological thermodynamics with internal variables, the present work has demonstrated the viability of development of models capable of accounting for effects of frictional wear damage in the finite-element analysis of practical industrial problems. In situations occurring typically in double sided contact between sheet and blank holder/die and in the draw bead region in deep drawing processes, the frictional behaviour is known to be of utmost importance in determining the success or failure of forming operations. In these cases, it is expected that the use of the model described in this paper, with appropriate experimental data, will produce more realistic numerical simulations.

E.A.S.N. thanks the Brazilian Council for Scientific and Technological Development – CNPq for the financial support received (Proc. No. 202455-89.0). The authors are indebted to Dr M. Usuda and Mr T. Yoshida, from Nippon Steel Co., who organized and carried out the experiments. We thank J. Yu for his involvement in the numerical implementation of the model presented in this paper.

References

Archard, J. P. 1986 Friction between metal surfaces. *Wear* **113**, 3–16.

Bay, N. & Wanheim, T. 1990 Contact phenomena under bulk plastic deformation conditions. In *Advanced technology of plasticity 1990: Proc. 3rd Int. Conf. on Technology of Plasticity*, pp. 1677–1691. The Japan Society for Technology of Plasticity.

Curnier, A. 1984 A theory of friction. *Int. J. Solids Struct.* **20**, 637–647.

Duvaut, G. & Lions, J. L. 1976 *Inequalities in mechanics and physics*. Academic Press.

Feijóo, R. & Fancello, E. A. 1992 An incremental kinematical formulation for the elastic-plastic contact problem with friction. In *Proc. 3rd Int. Conf. on Computational Plasticity: Fundamentals and Applications* (ed. D. R. J. Owen, E. Oñate & E. Hinton), pp. 375–393. Swansea: Pineridge Press.

Giannakopoulos, A. E. 1989 The return mapping method for the integration of friction constitutive relations. *Comput. Struct.* **32**, 157–167.

Hashimoto, K., Ohwue, T. & Takita, M. 1990 Effect of temperature, die material and lubricant on sliding behaviour of various coated steel sheets. In *Proc. 16th Int. Deep Drawing Research Group Congress*.

Hughes, T. J. R., Taylor, R. L., Sackman, J. L., Curnier, A. & Kanoknukulchai, W. 1976 A finite element method for a class of contact-impact problems. *Comp. Meth. Appl. Mech. Engng* **8**, 249–276.

Hutchings, I. M. 1992 *Tribology: friction and wear of engineering materials*. Kent: Edward Arnold.

Kikuchi, N. & Oden, J. T. 1988 *Contact problems in elasticity: a study of variational inequalities and finite element methods*. Philadelphia: SIAM.

Lin, J. F. & Wang, L. Y. 1992 Friction in deep drawing of aluminium sheet. *Wear* **156**, 189–199.

PHILOSOPHICAL TRANSACTIONS OF THE ROYAL SOCIETY A MATHEMATICAL, PHYSICAL & ENGINEERING SCIENCES

Lubliner, J. 1990 *Plasticity theory.* New York: Macmillan.

Michałowski, R. & Mróz, Z. 1978 Associated and non-associated sliding rules in contact friction. *Arch. Mech.* **30**, 259–276.

Mitchell, G. P. & Owen, D. R. J. 1988 Numerical solution for elasto-plastic problems. *Engng Comp.* **5**, 274–284.

Nakamura, Y., Nakamachi, E. & Wagoner, R. H. 1992 Deep drawing analysis of square cups with coated, rate-sensitive steel sheets. In *Proc. 3rd Int. Conf. on Computational Plasticity: Fundamentals and Applications* (ed. D. R. J. Owen, E. Oñate & E. Hinton), pp. 1301–1310. Swansea: Pineridge Press.

Oden, J. T. & Martins, J. A. C. 1985 Models and computational methods for dynamic friction phenomena. *Comp. Meth. Appl. Mech. Engng* **52**, 527–634.

Oden, J. T & Pires, E. B. 1983 Nonlocal and nonlinear friction laws and variational principles for contact problems in elasticity. *J. Appl. Mech.* **50**, 67–76.

Perić, D. & Owen, D. R. J. 1992 Computational model for 3-D contact problems with friction based on the penalty method. *Int. J. Numer. Meth. Engng* **35**, 1289–1309.

Perić, D., Owen, D. R. J. & Honnor, M. E. 1992 A model for finite strain elasto-plasticity based on logarithmic strains: computational issues. *Comp. Meth. Appl. Mech. Engng* **94**, 35–61.

Qiu, X. & Plesha, M. E. 1991 A theory for dry wear based on energy. *J. Tribol.* **113**, 442–451.

Rigney, D. A. & Hirth, J. P. 1979 Plastic deformation and sliding of metals. *Wear* **53**, 345–370.

Rockafellar, R. T. 1972 *Convex analysis.* Princeton University Press.

Simo, J. C. & Hughes, T. R. J. 1987 General return mapping algorithms for rate-independent plasticity. In *Constitutive laws for engineering materials: theory and applications* (ed. C. S. Desai *et al.*), pp. 221–231. Elsevier.

de Souza Neto, E. A., Perić, D. & Owen, D. R. J. 1993*a* A model for frictional contact with hardening: formulation and numerical implementation. *Tech. Rep.* CR/749/93. Department of Civil Engineering, University College of Swansea.

de Souza Neto, E. A., Hashimoto, K., Perić, D. & Owen, D. R. J. 1993*b* A phenomenological model for frictional contact of coated steel sheets. In *Proc. Numisheet 2nd Int. Conf.: Numerical Simulation of 3-D Sheet Metal Forming – Verification of Simulation with Experiment* (ed. A. Makinouchi, E. Nakamachi, E. Onãte & R. H. Wagoner).

Stein, E., Wriggers, P. & vu Van, T. 1989 Models of friction, finite element implementation and application to large deformation impact-contact problems. *Computational plasticity. II. Models, software and applications* (ed. D. R. J. Owen), pp. 1015–1041. Swansea: Pineridge Press.

Suh, N. P. & Sin, H. C. 1981 The genesis of friction. *Wear* **69**, 91–114.

Wriggers, P., Vu Van, T. & Stein, E. 1990 Finite element formulation of large deformation impact-contact problems with friction. *Comp. Struct.* **37**, 319–331.

Zhang, J., Moslehy, F. A. & Rice, S. L. 1991 A model for friction in quasi-steady sliding. 1. Derivation. 2. Numerical results and discussion. *Wear* **149**, 1–25.

Received 24 November 1993; revised 28 February 1995; accepted 25 May 1995

PHILOSOPHICAL TRANSACTIONS OF THE ROYAL SOCIETY A MATHEMATICAL, PHYSICAL & ENGINEERING SCIENCES

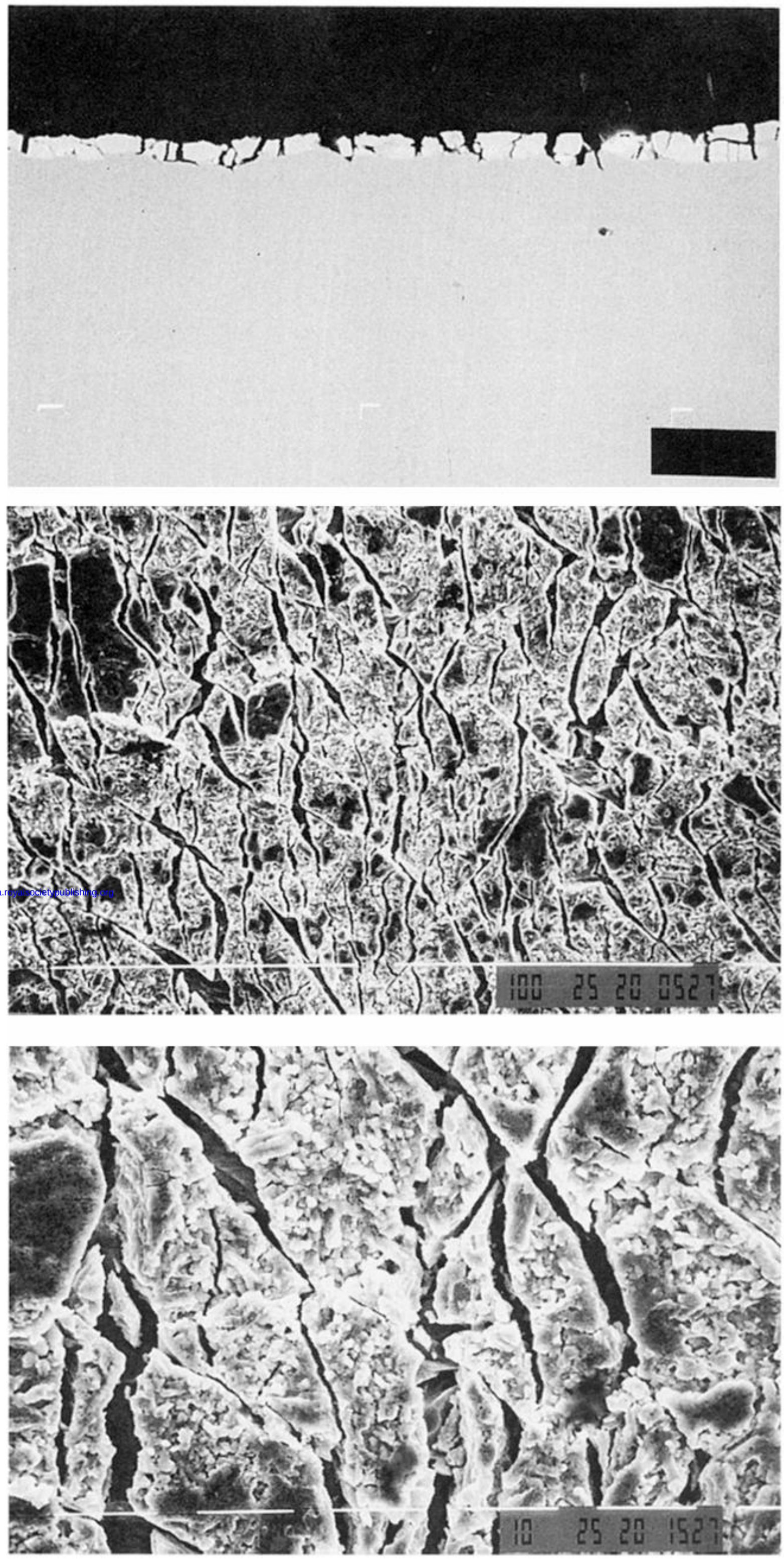

Figure 2. Galvannealed steel sheet: wall portion of hat channel product obtained under well-lubricated condition. SEM micrographs: (*a*) Cross section ×500, (*b*) outer surface ×500 and (*c*) outer surface ×1500.

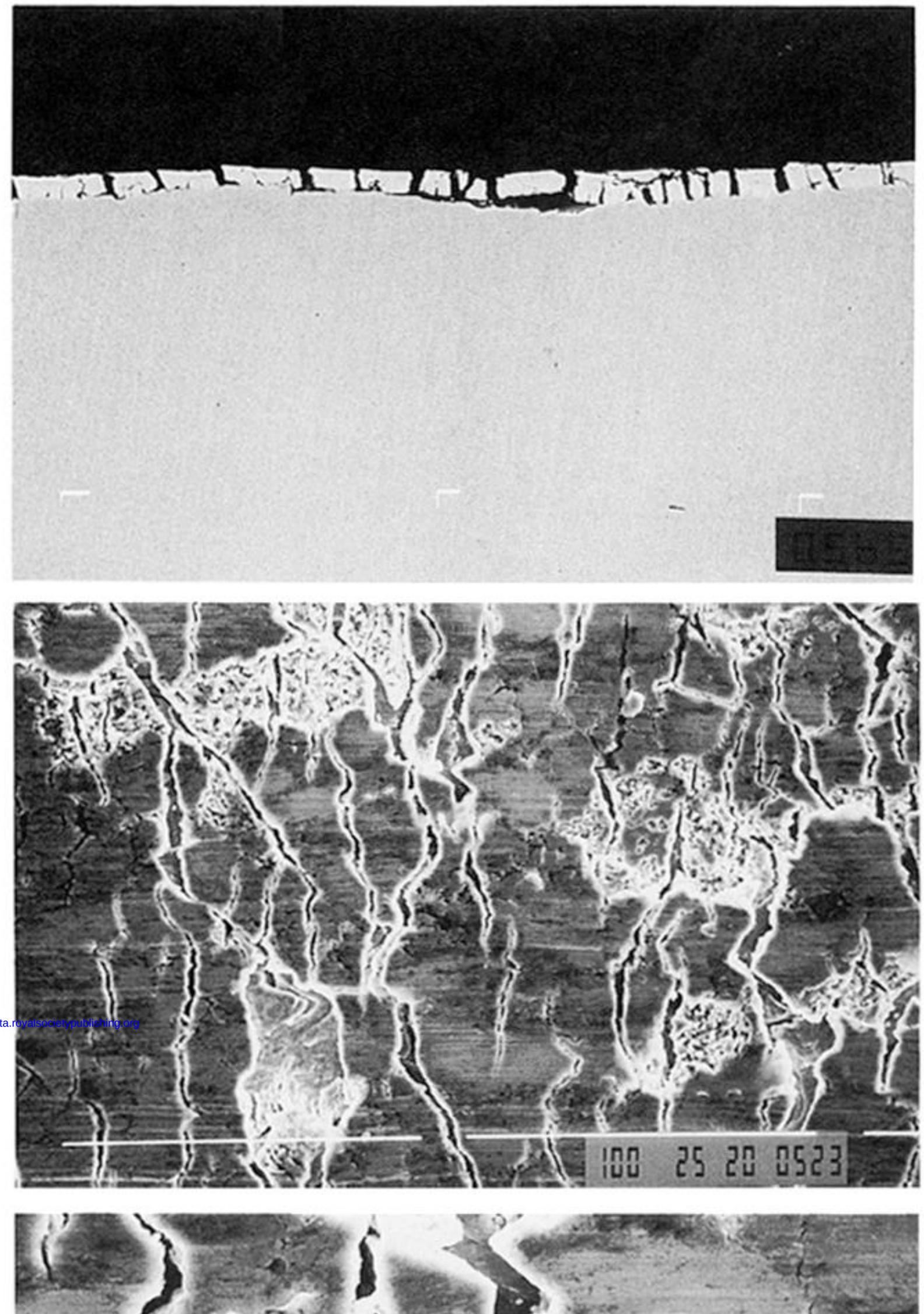

Figure 3. Galvannealed steel sheet: wall portion of hat channel product obtained under severe friction condition (degreased). SEM micrographs: (*a*) Cross section ×500, (*b*) outer surface ×500 and (*c*) outer surface ×1500.

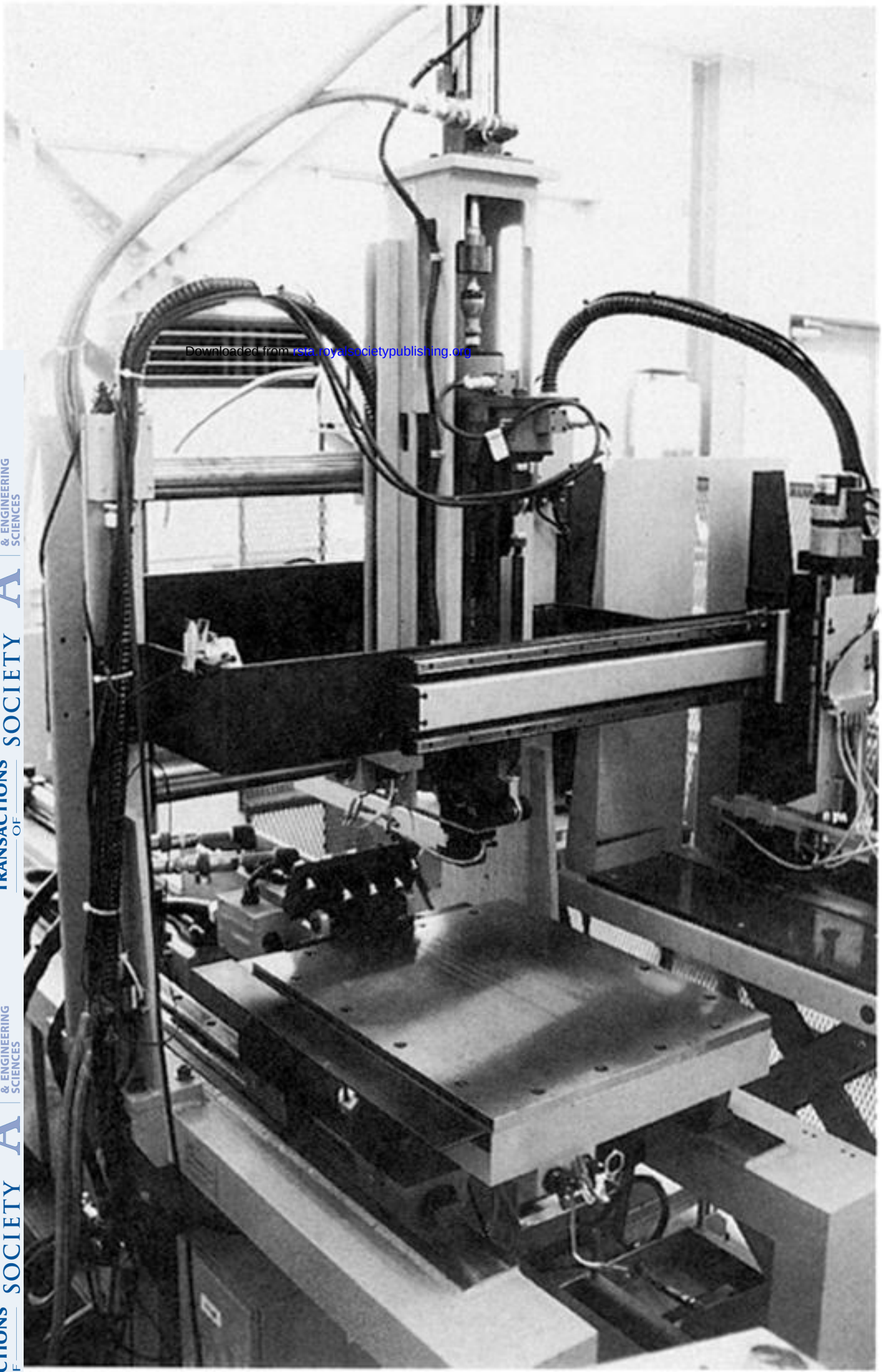

PHILOSOPHICAL TRANSACTIONS OF THE ROYAL SOCIETY A MATHEMATICAL, PHYSICAL & ENGINEERING SCIENCES

Figure 5. Flat sheet sliding machine.